Variability by region and method in human brain sodium concentrations estimated by 23Na magnetic resonance imaging: a meta-analysis

Ben Ridley, Filomena Morsillo, Wafaa Zaaraoui, Francesco Nonino

scientific reports

Check for updates

OPEN

Variability by region and method in human brain sodium concentrations estimated by ^{23}Na magnetic resonance imaging: a meta-analysis

Ben Ridley[1,4]✉, Filomena Morsillo[1], Wafaa Zaaraoui[2,3] & Francesco Nonino[1]

Sodium imaging (^{23}Na-MRI) is of interest in neurological conditions given potential sensitivity to the physiological and metabolic status of tissues. Benchmarks have so far been restricted to parenchyma or grey/white matter (GM/WM). We investigate (1) the availability of evidence, (2) regional pooled estimates and (3) variability attributable to region/methodology. MEDLINE literature search for tissue sodium concentration (TSC) measured in specified 'healthy' brain regions returned 127 reports, plus 278 retrieved from bibliographies. 28 studies met inclusion criteria, including 400 individuals. Reporting variability led to nested data structure, so we used multilevel meta-analysis and a random effects model to pool effect sizes. The pooled mean from 141 TSC estimates was 40.51 mM (95% CI 37.59–43.44; p < 0.001, $I^2_{Total=}$99.4%). Tissue as a moderator was significant (F^2_{14} = 65.34, p-val < .01). Six sub-regional pooled means with requisite statistical power were derived. We were unable to consider most methodological and demographic factors sought because of non-reporting, but each factor included beyond tissue improved model fit. Significant residual heterogeneity remained. The current estimates provide an empirical point of departure for better understanding in ^{23}Na-MRI. Improving on current estimates supports: (1) larger, more representative data collection/sharing, including (2) regional data, and (3) agreement on full reporting standards.

Sodium magnetic resonance imaging (^{23}Na-MRI) is of interest as a 'quantitative' imaging modality. Using a reference of known concentration (Fig. 1a), measured signal (M0) can be converted from arbitrary signal intensity to a quantitative scale (millimolars, mM). As a candidate for metabolic imaging in particular, the advantages of ^{23}Na-MRI include: (1) it natively produces 3D, whole-brain, voxel-based data and is not restricted to pre-defined volume-of-interest analyses, and (2) the fact it requires no contrast agents, meaning contraindications are the same as for conventional proton (^{1}H) MRI. Ionic homeostasis is a pre-requisite for proper cellular functioning, with sodium in the nervous system being critical in trans-membrane transport, osmotic and electrostatic regulation and the generation/propagation of action potentials[1–3]. As such, the non-invasive, in vivo measurement of sodium concentration by ^{23}Na-MRI is of interest in the context of neuro-oncological[4–6], neurodegenerative[7–9], demyelinating[10–19] and cerebrovascular[20] conditions, and in both physiological and pathological neuronal activity[21–25].

In practice, assigning a single imaging parameter to a voxel in an MRI image of biological tissue is an over-simplification. This is the case both for the weighted average referred to as 'total' or 'tissue sodium concentration' (TSC) in ^{23}Na-MRI, as well as 'conventional' MRI contrasts targeting tissue water protons (^{1}H) such as diffusion or T_2 measurements[26,27]. Image sampling/tissue fraction effects are one reason, where diverse tissue types such as white and grey matter (WM and GM) and cerebrospinal fluid (CSF) contribute to measured signal within a single voxel. Even within a given tissue type MRI cannot resolve the sub-cellular compartments/organelles that, in the case of ^{23}Na-MRI, can be said to actually have a specific concentration[28]. The measurement of a given

[1]IRCCS Istituto Delle Scienze Neurologiche di Bologna, Bologna, Italy. [2]Aix Marseille Univ, CNRS, CRMBM, Marseille, France. [3]APHM, Hôpital de La Timone, CEMEREM, Marseille, France. [4]Ben Ridley, Epidemiologia e Statistica, IRCCS Istituto Delle Scienze Neurologiche di Bologna, Padiglione G, Via Altura, 3, 40139 Bologna, Italy. ✉email: ben.ridley@ausl.bologna.it

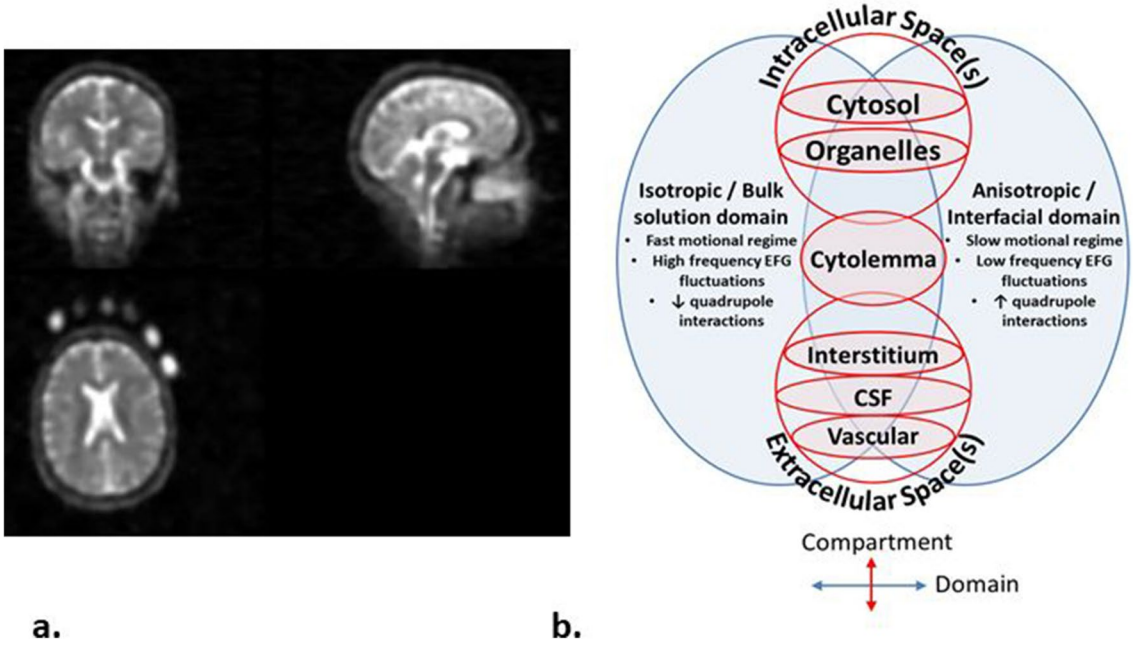

Figure 1. ^{23}Na magnetic resonance imaging. (**a**) An exemplar ^{23}Na-MRI brain image, with external calibration phantoms of differing concentrations visible on the bottom left axial image. Calibration can also be done relative to internal references such as vitreous humor or cerebrospinal fluid in the ventricles. (**b**) Schematic Venn diagram (following the nomenclature in Springer[28]) showing physical domains (Blue) where nuclei share similar nuclear magnetic resonance properties, and biological compartments (Red) found in brain tissue. These are arrayed along two axes to indicate their orthogonality: neither physical domain is unique to any given biological compartment. ^{23}Na-MRI TSC estimates are a weighted average influenced by concentrations, volumes and microstructure in a range of environments including the intracellular (neuronal and glial cytosol, and organelles), extracellular (interstitial and vascular spaces.) and membranous (cyto/axolemmal) contributions[28]. The vast majority of in vivo sodium is present in metal-aquo complexes with a tetrahedral hydration shell surrounding the ^{23}Na ion, with a much smaller population bound to macromolecular loci[80]. The domain on the left corresponds to the situation in bulk solution, where magnetic and electric fields average out to become isotropic. An anisotropic domain (right) pertains at the interface of/with macromolecules and/or lipid assemblies, where the surface experienced by a diffusing ion is not randomly orientated and the resulting electric field gradient (EFG) fluctuations do not average to zero. ^{23}Na is a quadropolar ion (spin = 3/2) that, under the influence of a magnetic field, exhibits four energy levels with three possible single quantum transitions, one central and two satellites each contributing to relaxation[81]. In the context of isotropic domains, *i.e.* aqueous environments with rapid motions, quadrupole interactions are minimal and all transitions occur approximately at the same decay time resulting in a MRI-visible monoexponential decay curve[81]. In anisotropic domains, where motions are slowed, the non-spherical distribution of the electric charge of the sodium nucleus permits interaction with anisotropic electric fields of the charged groups on the macromolecular anions. Thus, quadrupole interactions are non-zero and biexponential relaxation is observed[66,80–82] with the satellite transitions showing faster decay than the central transition.

voxel will include, at a minimum, intracellular and extracellular compartments with their own concentrations, volumes and microstructure (Fig. 1b).

Physical behaviour of sodium atoms in biological media and the complexities of measuring them with MRI present other challenges. Relative to tissue water protons, the lower MR sensitivity and abundance of ^{23}Na result in lower signal to noise ratios and larger voxel sizes, exacerbating tissue fraction effects[29,30]. ^{23}Na-MRI pulse sequences with ultra-fast echo times (TE) that compensate for the short, biexponential transverse relaxation of ^{23}Na nuclei[29–32], often use non-cartesian sampling schemes which can have broader point spread functions (PSF) and greater inter-voxel spill-over effects in comparison to ^{1}H-MRI. These partial volume effect (PVE) issues are the target of growing attempts to develop or import PVE correction techniques, such as those adapted from positron emission tomography imaging (PET)[12,29–32]. Correction techniques beg the question of benchmarks for correction algorithms to target.

A range of tissue volume models to understand and validate ^{23}Na-MRI-derived concentrations have been proposed. The 'canonical' model describes two compartments: a large volume/low concentration (variously 10–15 mM[5,6,10,20,33,34]) intracellular space and an extracellular space of smaller volume but higher concentration (140 mM[5,6,10,20] or 145 mM[33,34]). These figures lead to a general estimate for overall brain tissue (parenchyma) of about 37–45 mM[6,12,20]. Model-based estimates beyond a general figure for parenchyma or gross tissue divisions like GM or WM are largely lacking[35], particularly because the cellular data required to elaborate beyond this are for the most part not available. More broadly, histology is an invaluable tool but should not be naively taken as the absolute gold-standard for MR features both because it is not necessarily sensitive to the same properties as

MR[27] and because various techniques suffer from their own limitations regarding compartmental concentrations, ecological validity given preparation effects, and limited spatial, temporal and cross-species sampling[28].

The positioning of ^{23}Na-MRI as a putative 'quantitative' method, implies that concentration measures should converge toward a 'true' estimate for a given sample, modulo statistical and methodological effects. If ^{23}Na-MRI is sensitive to the physiological state of tissues—a key assumption motivating its use in the context of neurological conditions—regional variability in measured TSC concentrations should also be expected. Conversely, positing a single parenchymal concentration as sufficient to characterise all regions implies a limit on detectable differences between individuals with and without neurological conditions, given known variation in factors like fluid fractions[36,37], distributions of cellular types and architectures[38,39] and macromolecular content[40–42].

In this context, meta-analytic approaches are another means to synthesize evidence and identify impediments and progress towards consensus. Meta-analysis aims to estimate the true effect size (including central tendency measures like the mean) based on the combination of observed effect sizes taken from several empirical samples, while trying to account for sample and study variability[43]. As such, we sought to apply a meta-analytic approach to investigate the existing literature on estimates of TSC in human brain regions. We aimed to address (1) the range of available evidence in the form of regional TSC estimates in the literature, (2) the possibility of consensus estimates of concentration in various brain regions, and (3) the extent to which methodological and anatomical factors contribute to variation in measured TSC.

Results

Search results. A search (see Methods) of MEDLINE dated 12/7/2021 returned 127 records, and we identified an additional 278 records by examining the bibliographies of recovered records and the 'cited by' function on the PubMed website. These records underwent screening of titles and abstracts, and the remaining texts underwent full text assessment for inclusion (see Preferred Reporting Items for Systematic Reviews and Meta-Analyses (PRISMA) flow diagram Fig. 2, and Supplementary Tables 1, 2 for PRISMA checklists). From an overall total of 405 records, 44 records were screened from further consideration based on title/abstract. 361 records were sought for full text retrieval, of which 329 were excluded with the main reasons being a focus on non-brain tissue or the lack of a sodium measurement in the form of a concentration estimate. We were unable to access four records. See Supplementary Table 3 for a full list of records identified and reasons for exclusion. Inclusion criteria were met by 28 reports.

Included studies. We included 28 reports containing measurements of total sodium concentration in healthy controls of specified human brain regions or tissue divisions (other than 'parenchyma') (Table 1). Nominally, 400 healthy controls in total were included in these reports, the mean number per report being 14.3 individuals (range: 4–45, S.D: 11.1). All but three included reports were published after 2010 (Fig. 3a).

We used a modified version of the checklists associated with the Committee on Best Practice in Data Analysis and Sharing (COBIDAS)[44], appropriate to the context of ^{23}Na-MRI: specifically, the sections on descriptive statistics, image acquisition reporting and pre-processing reporting. A list of reporting domains included in the modified version can be found in Supplementary Table 4, along with the coded results from the included reports and a summary can be seen in Fig. 3b. Information relating to the numbers of included participants, whether informed consent was given, MRI scanner used, repetition time (TR), echo time (TE), pulse sequence and nominal resolution was provided by all included studies. No included report provided information of the distribution of handedness in the included groups. The remaining domains were reported by varying numbers of included reports.

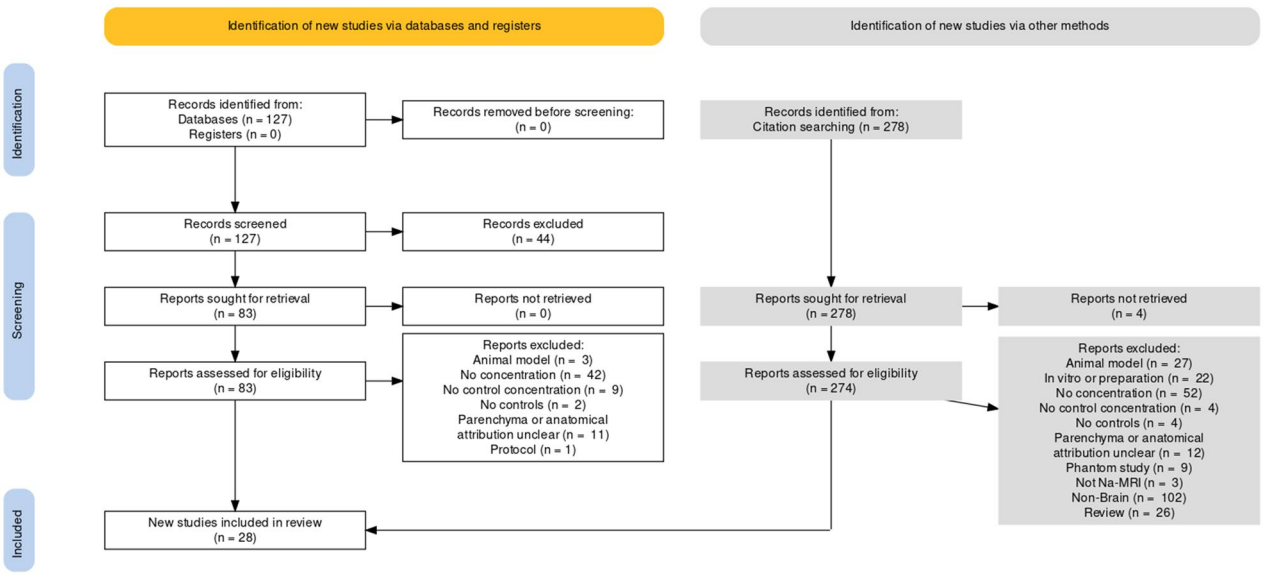

Figure 2. PRISMA flow diagram for search performed 12/7/2021. Generated with the PRISMA 2020 app[83].

Paper	Ref	Tesla	Sequence	Calibration[a]	TR[b] (ms)	TE[c](ms)	Voxel volume (mm^3)[d]	N	N. Female	Age (years)[e]	Comparison group
Winkler et al. 1989	45	1.5	GRE	Int. VH	98	3	490	4	NR	20–35	None
Ouwerkerk et al. 2003	5	1.5	TPI	External	120	0.37	39.3	9	3	22–63	Tumour
Thulborn et al. 2005	87	3	TPI	External	100	0.3	125	5	NR	NR	Stroke
Inglese et al. 2010	10	3	Radial	External	120	0.05	64	13	10	36.7, 26–60	MS
Lu et al. 2010	33	3	FlexTPI	External	160	0.36	125	5	1	32.4 ± 8.9	None
Reetz et al. 2012	8	4	SPRITE	External	10	0.3	64	13	6	44.9 ± 9.9	HD
Qian et al. 2012	71	7	AWSOS	Int. CSF	100	0.5	2.9	5	5	20–48	None
Zaaraoui et 2012	11	3	DA radial	External	120	0.2	46.6	15	12	30.20–54	MS
Paling et al. 2013	12	3	Radial	External	120	0.27	64	27	16	42.9 ± 11.3	MS
Maarouf et al. 2014	13	3	DA radial	External	120	0.2	46.6	15	NR	30, 21–54	MS
Mirkes et al. 2015	73	9.4	AWSOS	External	150	0.3	5	5	1	29 ± 4	None
Niesporak et al. 2015	88	7	DA radial	External	150	0.45	27	4	1	26 ± 2	None
Eisele et al. 2016	15	3	DA radial	External	60	0.22	46.6	10	5	33.23–53	MS
Petracca et al. 2016	16	7	GRE	External	150	6.8	125	17	8	46.16 ± 11.65	MS
Thulborn et al. 2016	34	9.4	FlexTPI	External	160	0.26	42.9	45	NR	48 ± 19	None
Maarouf et al. 2017	14	3	DA radial	External	120	0.2	46.7	31	15	35.7 ± 12.4	MS
Eisele et al. 2017	17	3	DA radial	External	60	0.22	46.7	6	5	42 ± 10	MS
Ridley et al. 2018	63	7	DA radial	External	120	0.3	42.9	13	5	23.9 ± 3.6	None
Worthoff et al. 2018	46	4	SISTINA	Int. VH	150	0.36	216	40	16	19–70	None
Reimer et al. 2019	72	3	Cones	External	100	0.5	64	11	3	32 ± 6	None
Driver et al. 2019	89	4.7	TPI	Int. VH	85	0.11	65.5	9	5	30 ± 6	None
Liao et al. 2019	90	3	TPI	Int. CSF	160	0.4	40.7	8	3	25–32	None
Meyer et al. 2019a	91	3	DA radial	External	120	0.2	46.7	12	8	31 ± 8.3	None
Meyer et al. 2019b	24	3	DA radial	External	120	0.2	64	12	12	34.3 ± 10.7	Migraine
Kim et al. 2020	32	7	GRE	Int. CSF	100	4	64	8	0	20–35	None
Gerhalter et al. 2021	92	3	FLORET	Int. VH	100	0.2	216	19	12	31.4 ± 7.5	TBI
Brownlee et al. 2019	19	3	Cones	External	120	0.22	27	34	23	35.5 ± 10.1	MS
Schneider et al. 2021	59	7	DA radial	Int. CSF	100	0.35	8	5	3	28.4 ± 6.5	None

Table 1. Characteristics of included studies. [a]*Int*. internal, *Ext*. external, *CSF* cerebrospinal fluid, *VH* vitreous humour (eyes). [b]Repetition time. [c]Echo time, where multiple the shortest TE was used in analysis. [d]x,y,z product of nominal resolution, see Supplementary Table 7 for specific values. [e]NR = not reported, other values are presented as per original reports in ranges (XX-XX), mean ± standard deviation, except for Zaaraoui et al. 2012 and Maarouf et al. 2014 which report median and range and Inglese et al. 2010 and Eisele et al. 2016 which report mean and range.

Descriptive. From the 28 included studies, a total of 162 effect sizes in the form of means and SD of measured TSC (mM) in healthy controls were extracted. In addition, relevant information relating to the COBIDAS domains for which all included studies had relevant data were extracted, except for 'Scanner' where the reporting was too variable and insufficient to permit reclassification. To account for variability in nomenclature, 'Pulse sequence' and 'Tissue' were re-coded according to Table 1 and Supplementary Table 5, respectively. Tissue re-coding was informed by the wish to maximise the data per region, tissue homogeneity and physiological plausibility and minimise non-independence, and we excluded twenty effect sizes from regions too sparsely sampled to satisfy these considerations. The remaining 141 effects sizes across 14 updated Tissue regions in were taken forward for meta-analysis (Fig. 3c): 22 effect sizes for both GM and WM regions; 14 in the Brainstem and Pons combined; 10 each in Central WM, Thalamus, and 'GM, Temporal' regions; eight each in 'Deep WM' and WM in the cerebellum and dentate nucleus (WM, Cb + DN); seven each in 'GM, Parietal' and Putamen; six each in Caudate, Globus Pallidus and 'GM, Frontal' and five in 'GM, Occipital'.

We also recorded the type of calibration method used—an external phantom, or internal references in the vitreous humour of the eyes or the ventricles of the brain. Since important demographic factors like age and sex were not completely reported COBIDAS domains (Fig. 3b), we also recorded 'Comparison group' in the hopes that this might capture some of the variability associated with missing demographic information. Where controls were selected based on matching for age and sex to a patient group, the characteristic range for these factors in certain patient groups could represent a sampling bias varying between conditions e.g. controls matched to patients with Huntingdon's disease versus multiple sclerosis. Reports without a patient-defined comparison group can often be technical MR methodology papers, which may tend to sample from a different population, such as for example the authors/students themselves.

Multi-level meta-analysis: model-fit. We used a multilevel/multivariable approach with four levels (participant, effect size, tissue regions and study), and a random effects model to pool effect sizes. The pooled

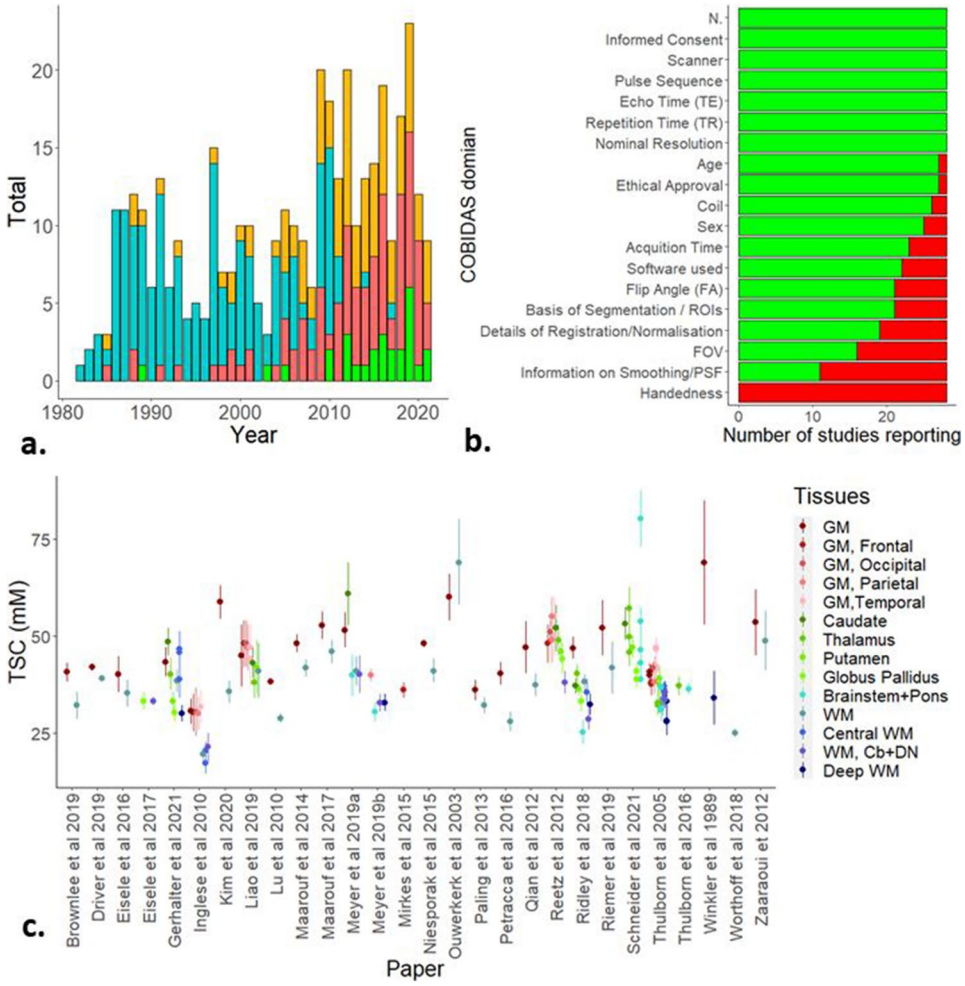

Figure 3. Descriptive plots for identified and included studies. (**a**) Literature search results 1980–2021 by year of publication. Chart includes total papers published for a given year (orange), publications identified by searching bibliographies (cyan), papers identified through the MEDLINE search (red) and number of studies included (green). (**b**) Overview of COBIDAS Domains reported in included studies. FOV, Field of view; PSF, Point spread function; ROIs, regions of interest. (**c**) Scatterplot of 141 effect sizes used in meta-analysis by published report in alphabetical order of first author surname. Error bars correspond to standard deviation, except for Zaaraoui et al. 2012 who reported range and Driver et al. 2019 who reported standard error. *Cb* cerebellum, *DN* dentate nucleus, *GM* grey matter, *WM* white matter. Images created in R[84–86].

mean of TSC across all 141 estimates based on the multilevel meta-analytic model was 40.51 mM (95% CI 37.59–43.44; $p < 0.001$). We identified considerable heterogeneity (I^2_{Total}=99.4%), with the results of the standard random-effects model suggesting that most of the total variance is due to between-study heterogeneity (i.e., variance in the 'true' means), while the remaining (0.6%) can be attributed to sampling variance.

Variance components: tissue and study factors. The factors Tissue and Study were included in the model to account for the nested structure of dependencies within the data: there are multiple effect sizes per paper and the effect sizes are not independent—a given individual may have contributed to multiple levels of the factor Tissue, and a given region may be estimated based on different numbers of effect sizes from multiple and varying numbers of papers. The estimated variance components were t = 45.81 for the Study level, 9.93 for Tissue level and 28.96 for Effect Size level. In terms of the distribution of variance across levels as a percentage of total variance, 53.75% of the total variation in our data can be attributed to between-study heterogeneity, 11.65% to between-tissue heterogeneity and 33.99% to the effect size level (i.e. within-factor heterogeneity for Tissue), and only 0.6% is due to sampling variance. The high heterogeneity both between Studies and within Tissue, suggest that a subgroup analysis by anatomical region is appropriate.

Model comparison: tissue sub-group versus reduced model. In Fig. 4 we report the forest plots for anatomical regions with at least ten effect sizes only (following general statistical power guidelines for meta-analytic sub-analyses[43]). These included (pooled mean [95% CI]): GM (45.92 mM [42.27; 49.57]), Temporal GM

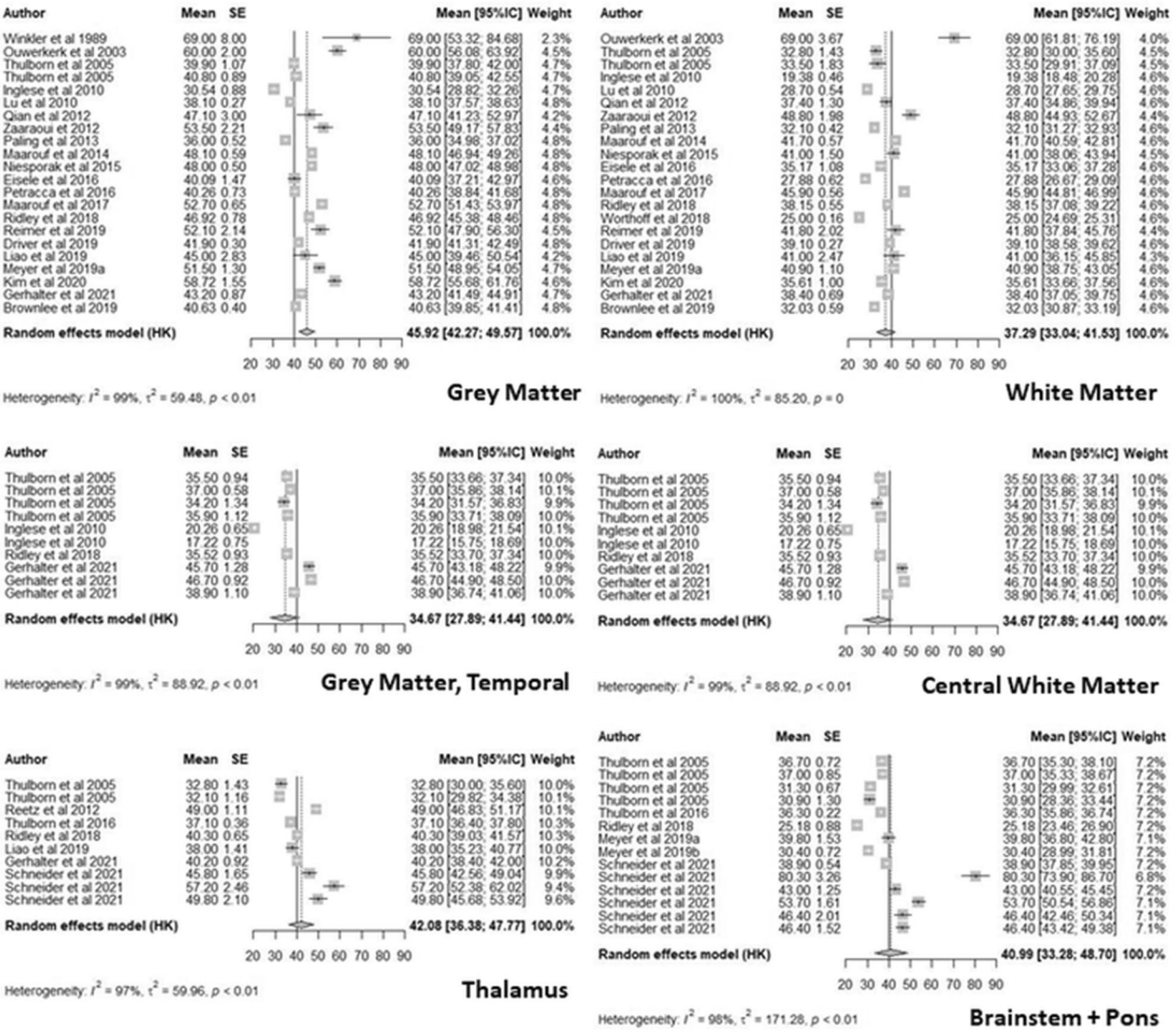

Figure 4. Forest plots for anatomical regions with at least ten effect sizes: grey matter; Temporal grey matter; thalamus; white matter; central white matter; brainstem + pons. Each forest plot contains the effect size data, represented by grey squares scaled to their weight in the meta-analytic model and error bars corresponding to 95% confidence intervals. The regional pooled estimate for each plot is represented by a grey diamond scaled in length to the confidence interval of the pooled estimates, and a dotted reference line. The pooled overall mean of all 141 included effect sizes is represented by a solid reference line on each plot. Plots generated in R, in the metafor package[74].

(45.48 mM [40.92; 50.05]), Thalamus (42.08 mM [36.38; 47.77]), Brainstem + Pons (40.99 mM [33.28; 48.70]), WM (37.29 mM [33.04; 41.53]) and 'Central' WM (34.67 mM [27.89; 41.44]). We found that the subgroup multilevel model provided a significantly better fit compared to a reduced multilevel model, as indicated by lower Akaike (AIC) and Bayesian Information Criterion (BIC). The likelihood ratio test (LRT) comparing both models is significant ($\chi^2_{13} = 145.50$, $p < 0.01$). A test of the moderators 'Tissue' was significant, $F^2_{14} = 65.34$, p-val < 0.01), indicating that in this model the mean TSC is different between each anatomical region. However, the results indicate that high heterogeneity remains overall even with the inclusion of 'Tissue' level ($\chi^2_{127} = 9537.26$, p-val < 0.01).

Precision, small study effects and publication bias. We investigated further factors impacting the distribution of results with respect to pooled means via Egger's tests and funnel plots (Fig. 5). The egger's test used standard error, a measure of precision, as predictor. Things being equal, there should an inverse relationship between standard error and the probability of a given study's estimate being different from the actual value in the population, with an expected symmetry in over- and under-estimates. Overall, the distribution of all effect sizes did not show the expected distribution, showing substantial asymmetry (Egger's test, $t = 5.24$, $p < 0.001$) which remained statistically significant when outliers (identified by sensitivity analysis eliminating one by one the extreme points of the distribution) are removed ($t = 4.89$, $p < 0.001$). Asymmetry can be evidence for small study

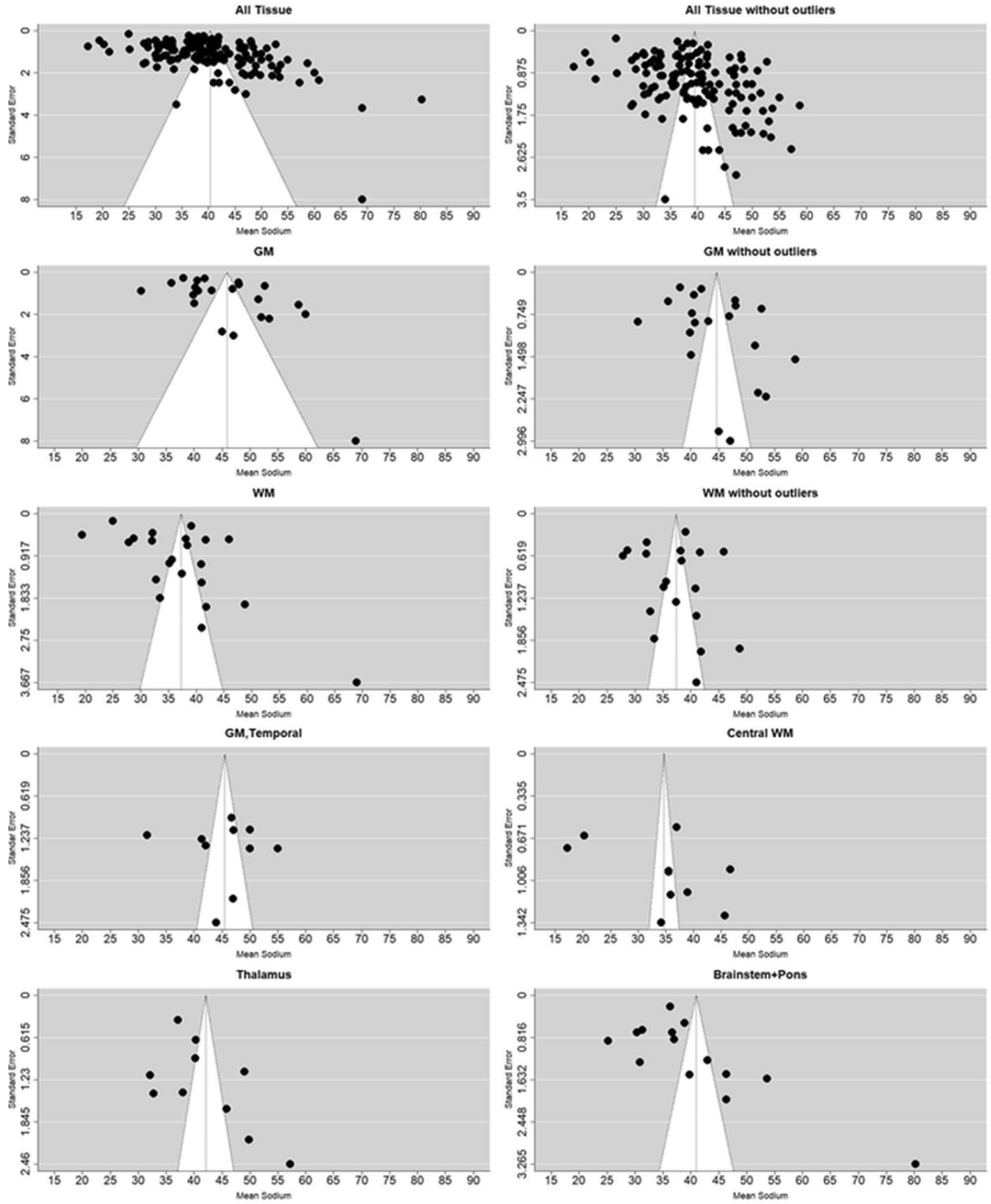

Figure 5. Funnel plots comparing effect sizes (mean TSC) with their precision (standard error): All tissues (141 effect sizes) and with outliers removed (136 effect sizes); GM effect sizes with (22, left) and without outliers (20, right); WM effect sizes with (22, left) and without outliers (19, right); GM, Temporal; Thalamus; Brainstem + Pons, and Central WM. Images created in R[74,84].

effects and publication bias, based on the assumption that small studies are at greatest risk of non-significant results and biasing the published literature toward the high effect sizes that are most likely to be significant with

small N[43]. In our case we are investigating a measure of central tendency: mean TSC, as opposed to a standardized mean *difference,* compared to standard error. As such, we investigated the possibility that our data does not show the expected symmetry because it is constituted by sub-groups, and the 'pooled mean' is not the best reference given the subgroup analysis, above.

In GM the test of asymmetry was at the threshold of significance ($t = 2.1$, $p = 0.05$), though after removing some outliers (60 mM[45]; 69 mM[5]) the figures become more symmetrical and the tests become non-significant ($t = 1.73$, $p = 0.1$) and the remaining regions do not show significant skewness. Similarly, in WM the presence of asymmetry is indicated ($t = 2.48$, $p = 0.02$), but after removal of some outliers (19.38 mM[10], 25 mM[46], 69 mM[5]) distribution was no longer significantly asymmetrical. The remaining regions did not show significant asymmetry.

Effect of moderators. Papers differed in their methodology across domains. We sought to understand the effect of additional methodological moderators by adding them individually and exploring their association with different mean TSC estimates. Relative to a reduced model including the factor Tissue, all additional individual factor added to the model produced a significantly better fit (Table 2), in terms of reducing overall heterogeneity.

Moderator effects on mean TSC. Within factors, we explored the levels associated with significant differences in mean TSC between levels independent of Tissue (Fig. 6). For studies using Sequence Type as "Radial" or "SISTINA", the mean TSC is significantly lower than that of studies using the "DA Radial" type ($t_{118} = -2.95$, $p < 0.01$ and $t_{118} = -2$, $p < 0.05$ respectively). Field strength of 1.5 T is associated with higher concentrations of Sodium ($t_{122} = 2.54$, $p = 0.01$) relative to 3 T. In studies with "Brain Tumour" as the Comparison Group the mean TSC is higher in controls ($t_{118} = 2.68$, $p < 0.01$) than in studies where there was no comparison group. A single study is sampled for the SISTINA level of the factor Sequence while another single study was sampled both at the 1.5 Tesla level of the factor Field Strength and the Brain Tumour level of Comparison Group, which was also identified as an outlier in the assessment of asymmetry in standard error distribution for both GM and WM[5] (Figs. 5, 6). Tests for Calibration method, Voxel Volume, TR and TE were non-significant, indicating no association between the level of the two moderators and the mean measured sodium level, regardless of region.

Intra-regional heterogeneity. Given the high heterogeneity within the factor Tissue, we extended our analysis to identifying where inclusion of methodological moderators reduces the heterogeneity of estimates within anatomical regions (with at least 10 effects sizes) suggesting the pooled estimates in the reduced model are impacted by differences in a given factor. We compared the specific heterogeneity (tau) of a region in the reduced model compared to the model with the methodological factor using Hedges' g, identifying 'significant' reductions in the form of a standardized mean difference whose 95% CIs did not cross zero (Supplementary Table 6, Supplementary Fig. 1).

'Sequence' as moderator reduces the heterogeneity for GM, GM-Temporal and WM regions. Adding "Comparison Group" reduces heterogeneity in GM, Brainstem + Pons, and WM. "Calibration method" reduces heterogeneity within GM. Residual heterogeneity is reduced in "Brainstem + Pons" when "Voxel Volume" is used as a moderator. "TR" reduced residual heterogeneity when used as a moderator in Temporal GM and the thalamus. "TE" reduced heterogeneity in Temporal GM and Central WM. Field strength did not contribute to explaining the variability within anatomical regions. Note that for all methodological factors, the test of residual heterogeneity for the model overall remained significant (Table 2).

Discussion

Data from 28 studies, identified by literature search, were explored via meta-analysis—to our knowledge the first such attempt in the context of data from ^{23}Na-MRI. The overall pooled estimate from all 141 across all 28 studies was 40.51 mM (95% CI 37.59–43.44), well within the ranges suggested by parenchymal volume models (37–45 mM[6,12,20]). Meta-analytic estimates were associated with high heterogeneity, which further analysis suggested was largely associated with between-study heterogeneity. This supports the idea that there is underlying differences in the 'true means' the different studies are trying to measure—and that a parenchymal estimate is not sufficient to characterise the range of empirical values obtained from different brain regions. Pooled estimates

	Likelihood ratio test			Test of residual heterogeneity		
Moderator	DF	χ^2	*p*	DF	χ^2	*p*
Sequence	9	78.07	< 0.01	118	4772.90	< 0.01
Comparison group	6	50.73	< 0.01	121	9081.33	< 0.01
Calibration method	2	16.82	< 0.01	125	8636.05	< 0.01
Voxel volume	1	7.93	< 0.01	125	7963.39	< 0.01
Field strength (Tesla)	5	26.81	< 0.01	126	9216.67	< 0.01
Repetition time (TR)	1	29.74	< 0.01	126	8697.18	< 0.01
Echo time (TE)	1	16.01	< 0.01	126	9529.9	< 0.01

Table 2. Tests comparing models including each methodological moderator to a reduced model. *DF* degrees of freedom.

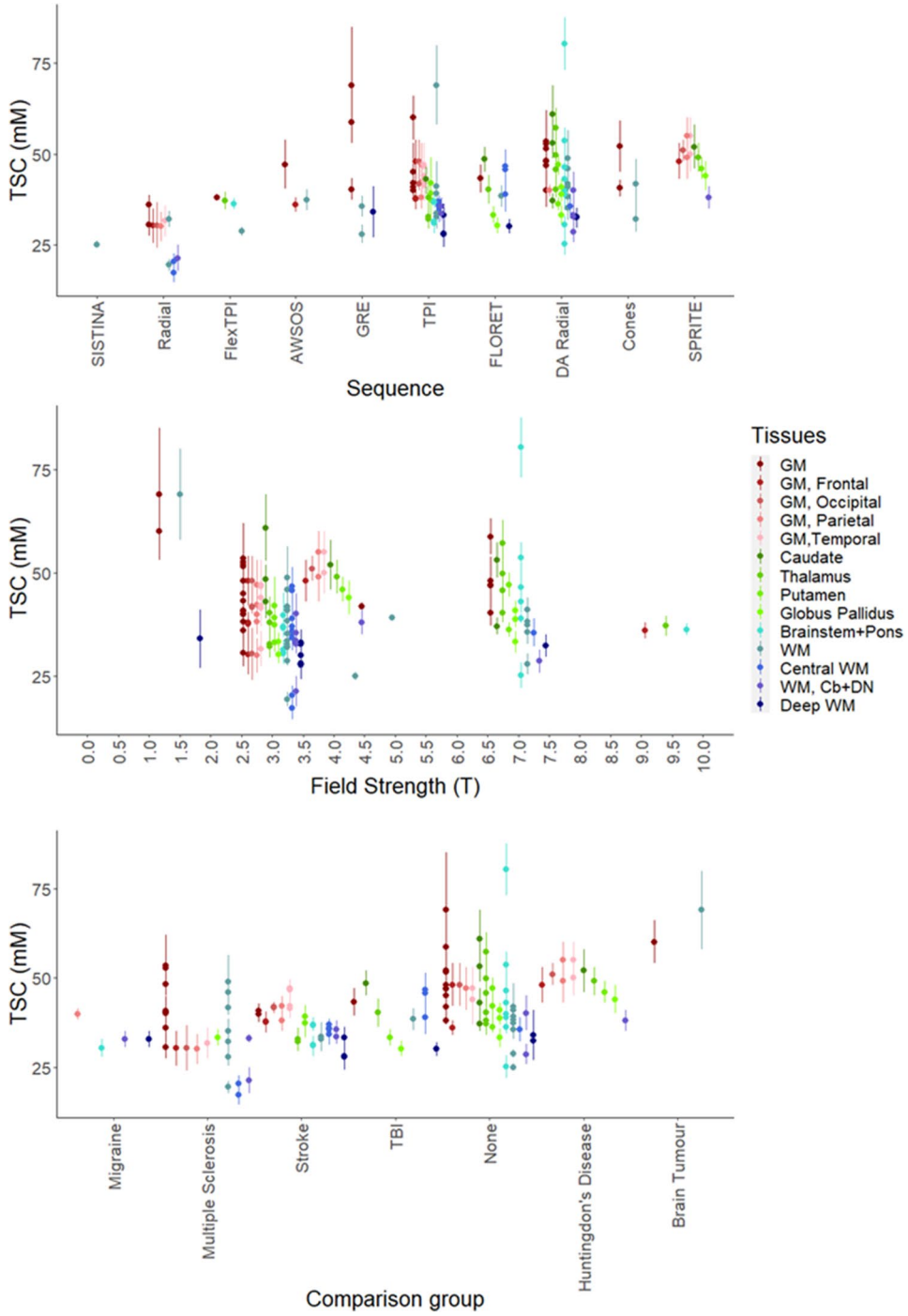

Figure 6. Scatterplot of 141 effect sizes used in meta-analysis ordered by moderators with a mean effect on TSC between levels independent of Tissue. Error bars correspond to standard deviation, except for Zaaraoui et al. 2012 (DA Radial, 3 Tesla, Multiple Sclerosis) who reported range and Driver et al. 2019 (TPI, 4.7 Tesla, None) who reported standard error. Cb, cerebellum, *DN* dentate nucleus, *GM* grey matter, *WM* white matter. Images created in R[84–86].

based on the extant literature of TSC estimates in human samples are 45.92 mM [42.27; 49.57] for GM and 37.29 mM [33.04; 41.53] for WM. This is noticeably higher than tissue volume model-based estimates for both tissue types, with examples including estimates of 20–33 mM in WM and for 30–35 for GM[33,47].

A number of potential sources may account for discrepancy between theoretical tissue volume models and the empirical estimates. One is partial volume effects, and other methodological factors impacting acquisition of the estimates making up the literature explored here. The models use simplifying assumptions, most notably that they have adequately captured the relevant influences on sodium ^{23}Na-MRI measurement with a limited

number of compartmental volume contributions, and that these compartments are internally homogenous. For example, the extracellular compartment is generally (but not always[35]) considered to include everything outside cells membranes, thereby subsuming the interstitial extracellular matrix[48] and vascular spaces and attributing the ^{23}Na concentration of 'pure' CSF to the entire compartment[20,33,35,49]. Similarly, the contribution of membranes, lipids like myelin and other 'solids' are assumed to be captured by a single volume contribution with no sodium contribution (on the basis they exclude sodium and should reduce overall measured signal for a given volume[35,49]), and can be summarised by a single fractional variable (e.g. 0.7–0.9[33,35,37]) for a given tissue type. It would be interesting to see how the modification of any or all these foctors impacts interact to produce expected values and how this might be applied to regional estimates.

More granular tissue models are currently lacking, as the requisite cellular data is not available. A potentially relevant factor is regional variation in the ratios of different cell types in the context of divergent sodium concentrations, for example astrocytes have approximately twice the cytosolic sodium concentration (~ 15–20 mM) compared to neurons (~ 10 mM) in rodent samples[50–54]. Recent automated immunocytochemical techniques have provided much needed information, including correcting widespread misconceptions about neuronal versus non-neuronal populations and masses, however precise data on cell volumes and their variation—which would be relevant for building regionally specific volume models for ^{23}Na-MRI—are not yet available[38,39]. In the absence of complete histologic information, another source of insight could come from comparing ^{23}Na-MRI to other imaging indices that might capture relevant features, with other quantitative imaging modalities being of particular interest. Parallel changes in ^{23}Na-MRI measures and diffusion imaging[15,55–57] and proton density[58] are suggestive, but extending these to direct evaluations of the redundancy and complementarity with other quantitative modalities[59], especially in healthy controls, in a range of regions and tissue structures would be a welcome development.

While the empirical values are higher than the model-based estimates for a given tissue, the relative values of different tissue's concentrations (e.g. GM > WM) is preserved. The difference in myelin content between grey and white matter—captured in the differences in the solid fractions that are usually assigned—may account for some of this difference. Indeed, among the subcortical regions we were able to provide pooled estimates for (> 10 effect sizes), it is noticeable that intermediate values were produced. The ostensibly GM nucleus though highly myelinated Thalamus has a lower value (42.08 mM [36.38; 47.77]) than some other GM estimates (45.48 mM [40.92; 50.05] for Temporal, GM), while ROIs sampling regions that are likely to be predominantly WM but with contributions from GM nuclei like the brainstem and pons indicate higher values (40.99 mM [33.28; 48.70]) than some other regions (34.67 mM [27.89; 41.44] for 'Central WM'). While the overlap between confidence intervals and the remaining heterogeneity limits the certainty of these precise pooled means, which should not be taken as definitive given the limitations of the available literature as represented in this meta-analysis, the importance of considering the variation in apparent ^{23}Na associated with regional differences is reflected in the significant improvement in the model when including the tissue factor and the finding of significant differences in mean TSC between levels/regions.

Given the remaining unexplained heterogeneity even after the Tissue factor was involved, we explored additional methodological factors where full reporting made this possible. The fundamentally most limiting property of ^{23}Na-MRI is the reduced nuclear MR sensitivity and relative abundance of sodium and other non-^{1}H based contrasts[60], leading to reduced signal to noise ratios and resolution, and consequently to partial volume effects. A given 'Sequence' is an attempt mitigate between trade-offs in acquisition parameters with impacts on available signal and resolution (e.g. TE, TR, Flip angle, Voxel Volume, Field Strength). For example, the ideal sequence would entail a spin density weighting with a minimum of relaxation effects, however in practice studies will differ in the degree they are affected by T1 or T2 weighting and thus vary in quantification. Different internal and external calibration methods provide scope for different degrees of experimenter error as well as spatial and physiological variability[61]. Comparison group may reflect demographic factors of potential relevance[62] reflecting the target patient group and other variable experimenter/location factors.

We were unable to consider the majority of the methodological and demographic factors sought by the modified COBIDAS checklist because the information was not reported (Fig. 3b). Explicit reference to and information pertaining to the following COBIDAS domain were not identified for age, handedness, sex, coil information, acquisition time, processing software used, flip angle, segmentation and ROI definition, details of normalisation/registration, field of view, information pertaining to smoothing or point spread function. Working towards consensus reporting standards could facilitate comparability of studies in the future. The COBIDAS standards in general, and the adapted subset used here (Fig. 3, Supplementary Table 4) could represent a starting point, to which further ^{23}Na-MRI specific parameters could be added such as relaxation and B1 correction methods, as well as phantom calibration.

We found each fully-reported methodological factor with included beyond tissue improved the meta-analytic model fit (Table 2), but that significant residual heterogeneity remained regardless. Only Field Strength, Sequence, and Comparison Group differed in mean TSC between specific levels independently of tissue. Interpretations of these results should take into consideration the risk of bias due to sampling issues given the limited data for various levels of these factors. Considered in combination with Tissue, all methodological factors except for Field Strength reduced heterogeneity in some regions when included (Supplementary Fig. 1). Collectively these results stress the importance of methodological factors but also the limitations of the available literature and underline the need for more and completely reported data covering multiple acquisition schemes and brain regions.

We analysed estimates of Total/Tissue Sodium Concentration, as the most common measure available. Other ^{23}Na-MRI derived metrics are possible, for example there are approaches that measure[63] or filter sodium signal based on relaxation behaviour (e.g. inversion recovery, IR[64]), or multiple quantum filtering (MQF)[16]. In principle, any *specific* measurement of in vivo sodium by ^{23}Na-MRI—TSC, IR, MQF or other – cannot be said to derive from a single cellular-level tissue compartment[65]. However, while attribution to different sources is a subject

of longstanding and ongoing investigation[3,66,67], it is legitimate to discuss a *difference or change* in measured parameters (between conditions and across spatial/temporal domains) in terms of changes in concentration or structure in sub-compartments that may have contributed, even when the latter are below the limit of resolution. In practice, precisely attributing changes in empirical MR-level estimates to compartmental micro-features is unlikely to be definitive because these factors rarely alter in isolation. For example, while pathological TSC alterations may be related to metabolic impairments of transmembrane ^{23}Na exchange, they may also reflect changes in cellular death, swelling, proliferation etc[68–70]. Fundamentally, ^{23}Na-MRI appears to be a more sensitive than specific measure, and a claim that it is sensitive to variation in a particular structural, functional or patho-/physiological context is an empirical question to answered by further appropriate data and not modelling nor a priori arguments from incomplete biophysical data alone.

Some further limitations should be noted and considered in future analysis. Variable reporting required accommodations to be made in several factors that were included in the analysis. Allocation of a given data point to a particular level of Tissue was based on explicit textual references in the included studies, but the method of segmentation, precise anatomic boundaries, use of atlases and precise coordinates were not always clear. This may be another source of heterogeneity in the results, and again highlights the need for clear reporting. We also considered only published reports, and not 'grey literature' (e.g. dissertations, preprints, government reports, or conference proceedings)[43] which could potentially improve sampling. We produced and examined a central tendency measure via mean estimates of TSC, but if sufficient data were available meta-analytic analysis could be applied to other ^{23}Na-MRI metrics as well as combined estimates of differences between groups, structures, and states. Finally, we considered the impact of methodological parameters in isolation, while to fully characterise their impact it will likely be necessary to investigate their interactions.

Conclusions

Data from 28 studies, identified by literature search, were explored via meta-analysis—to our knowledge the first such attempt in the context of data from ^{23}Na-MRI. The nested nature of the data, due in part to accommodations made to the variability of reporting in the published studies, lead to the use of a multi-level meta-analytic approach. We produced pooled meta-analytic estimates of brain TSC, but significant remaining heterogeneity limits the certainty and precision associated with the estimates. Consideration of tissue differences explains part of that heterogeneity, but not all. Where they were fully reported, methodological moderators were explored. While their inclusion reduces heterogeneity within certain tissue regions, and effects the measured TSC levels, substantial residual heterogeneity remains. The current estimates provide an empirical point of departure for better understanding of variability in ^{23}Na-MRI. Improving on current estimates supports: (1) larger, more representative data collection/sharing, including (2) regional data, and (3) agreement on full reporting standards.

Methods

Literature search. The following MEDLINE search was run by BR via pubmed.ncbi.nlm.nih.gov on 12/07/2021: "Brain" [Title/Abstract] AND ((((sodium MRI [Title/Abstract]) OR 23Na MRI [Title/Abstract]) OR sodium imaging [Title/Abstract]) OR 23Na imaging [Title/Abstract])". Bibliographies of potentially eligible studies were consulted and studies of potential relevance to ^{23}Na-MRI were included in the screening.

Recovered records were excluded based on the abstract or full text if they were non-experimental, non-original reports (review/commentary), conference proceedings, phantom-only studies, concerned with cultured tissue or organs other than the brain, non-human subjects, or did not include estimates of sodium concentrations determined by quantitative ^{23}Na-MRI in healthy subjects without known neurological conditions. Studies considering only estimates in overall parenchyma, or where it was not possible to attribute estimates to a specified anatomical region were also excluded. Screening and full text review were performed by BR with reference to other authors as necessary.

Data extraction. Initial extraction of data pertaining to ^{23}Na-MRI concentrations and methodological domains was performed by BR, with verification and consultation with WZ. Data re-coding, as discussed in the "Descriptive" section in Results, was based on consensus decisions by WZ/BR for "Sequence" and FN/BR for "Tissue" (See Table 1 and Supplementary Table 5). Where a given study included multiple potentially relevant samples a context-based decision was made: where the same individuals were sampled with differing methods we took the highest field / highest resolution observation for Qian et al.[71]; where the same individual was sampled multiple times with the same methods (reproducibility studies) we took the overall mean across samples for Riemer et al.[72] and Meyer et al.[24]; where PVC-corrected values by different methods were used in Kim et al.[32] we used the spill-over and ventricular CSF-based PVC-corrected values. Where multiple TEs were reported[45,63,73] we used the acquisition with the fastest TE.

Meta-analysis. Meta-analyses were conducted in R (**R-4.1.2**) using the "metafor" package[74]. The restricted maximum likelihood estimator[75] was used to calculate the heterogeneity variance ($\tau 2$) and we used Knapp-Hartung adjustments[76] to calculate the confidence interval around the pooled effect. Multi-level models were investigated to account for any correlations induced by the multi-level structure of the data, whereby a given individual may have contributed to multiple levels of the factor Tissue, and a given region may be estimated based on different numbers of effect sizes from multiple and varying numbers of papers. To account for correlated sampling errors due to different effect sizes being based on the same sample of patients we used a Correlated and Hierarchical Effects (CHE) model[77]: an extension of the multilevel model that considers the correlation of effect sizes within clusters, in this case the factor 'Paper'. A robust Sandwich covariate estimator was used to

estimate confidence intervals and relative p-values[78]. Egger's tests[79] were used to evaluate asymmetry of funnel plots, based on weighted regression models with multiplicative dispersion, with standard error as the predictor.

Data availability

All data generated or analysed during this study are included in this published article and its Supplementary Information files.

Received: 4 November 2022; Accepted: 21 February 2023
Published online: 24 February 2023

References

1. Madelin, G. & Regatte, R. R. Biomedical applications of sodium MRI in vivo. *J. Magn. Reson. Imaging JMRI* **38**, 511–529 (2013).
2. Chatton, J.-Y., Magistretti, P. J. & Barros, L. F. Sodium signaling and astrocyte energy metabolism. *Glia* **64**, 1667–1676 (2016).
3. Thulborn, K. R. Quantitative sodium MR imaging: A review of its evolving role in medicine. *Neuroimage* **168**, 250–268 (2018).
4. Leslie, T. K. *et al.* Sodium homeostasis in the tumour microenvironment. *Biochim. Biophys. Acta Rev. Cancer* **1872**, 188304 (2019).
5. Ouwerkerk, R., Bleich, K. B., Gillen, J. S., Pomper, M. G. & Bottomley, P. A. Tissue sodium concentration in human brain tumors as measured with 23Na MR imaging. *Radiology* **227**, 529–537 (2003).
6. Thulborn, K. R., Davis, D., Adams, H., Gindin, T. & Zhou, J. Quantitative tissue sodium concentration mapping of the growth of focal cerebral tumors with sodium magnetic resonance imaging. *Magn. Reson. Med.* **41**, 351–359 (1999).
7. Grapperon, A.-M. *et al.* Quantitative brain sodium MRI depicts corticospinal impairment in amyotrophic lateral sclerosis. *Radiology* **292**, 422–428 (2019).
8. Reetz, K. *et al.* Increased brain tissue sodium concentration in Huntington's Disease—A sodium imaging study at 4 T. *Neuroimage* **63**, 517–524 (2012).
9. Mohamed, S. A. *et al.* Evaluation of sodium (23Na) MR-imaging as a biomarker and predictor for neurodegenerative changes in patients with Alzheimer's disease. *Vivo Athens Greece* **35**, 429–435 (2021).
10. Inglese, M. *et al.* Brain tissue sodium concentration in multiple sclerosis: A sodium imaging study at 3 tesla. *Brain J. Neurol.* **133**, 847–857 (2010).
11. Zaaraoui, W. *et al.* Distribution of brain sodium accumulation correlates with disability in multiple sclerosis: A cross-sectional 23Na MR imaging study. *Radiology* **264**, 859–867 (2012).
12. Paling, D. *et al.* Sodium accumulation is associated with disability and a progressive course in multiple sclerosis. *Brain J. Neurol.* **136**, 2305–2317 (2013).
13. Maarouf, A. *et al.* Topography of brain sodium accumulation in progressive multiple sclerosis. *Magma N. Y. N* **27**, 53–62 (2014).
14. Maarouf, A. *et al.* Increased total sodium concentration in gray matter better explains cognition than atrophy in MS. *Neurology* **88**, 289–295 (2017).
15. Eisele, P. *et al.* Heterogeneity of acute multiple sclerosis lesions on sodium (23Na) MRI. *Mult. Scler. Houndmills Basingstoke Engl.* **22**, 1040–1047 (2016).
16. Petracca, M. *et al.* Brain intra- and extracellular sodium concentration in multiple sclerosis: A 7 T MRI study. *Brain J. Neurol.* **139**, 795–806 (2016).
17. Eisele, P. *et al.* Sodium MRI of T1 high signal intensity in the dentate nucleus due to gadolinium deposition in multiple sclerosis. *J. Neuroimaging Off. J. Am. Soc. Neuroimaging* **27**, 372–375 (2017).
18. Grist, J. T. *et al.* Imaging intralesional heterogeneity of sodium concentration in multiple sclerosis: Initial evidence from 23Na-MRI. *J. Neurol. Sci.* **387**, 111–114 (2018).
19. Brownlee, W. J. *et al.* Cortical grey matter sodium accumulation is associated with disability and secondary progressive disease course in relapse-onset multiple sclerosis. *J. Neurol. Neurosurg. Psychiatry* **90**, 755–760 (2019).
20. Thulborn, K. R., Gindin, T. S., Davis, D. & Erb, P. Comprehensive MR imaging protocol for stroke management: Tissue sodium concentration as a measure of tissue viability in nonhuman primate studies and in clinical studies. *Radiology* **213**, 156–166 (1999).
21. Bydder, M. *et al.* Dynamic 23Na MRI - A non-invasive window on neuroglial-vascular mechanisms underlying brain function. *Neuroimage* **184**, 771–780 (2019).
22. Gandini Wheeler-Kingshott, C. A. M. *et al.* Challenges and perspectives of quantitative functional sodium imaging (fNaI). *Front. Neurosci.* **12**, 810 (2018).
23. Ridley, B. *et al.* Brain sodium MRI in human epilepsy: Disturbances of ionic homeostasis reflect the organization of pathological regions. *Neuroimage* **157**, 173–183 (2017).
24. Meyer, M. M. *et al.* Cerebral sodium (23Na) magnetic resonance imaging in patients with migraine—A case-control study. *Eur. Radiol.* **29**, 7055–7062 (2019).
25. Azilinon, M. *et al.* Combining sodium MRI, proton MR spectroscopic imaging, and intracerebral EEG in epilepsy. *Hum. Brain Mapp.* https://doi.org/10.1002/hbm.26102 (2022).
26. Dowell, N. & Wood, T. T2: Transverse relaxation time. In *Quantitative MRI of the Brain: Principles of Physical Measurement* 83–96 (CRC Press, 2018). https://doi.org/10.1201/b21837-6.
27. Novikov, D. S., Kiselev, V. G. & Jespersen, S. N. On modeling. *Magn. Reson. Med.* **79**, 3172–3193 (2018).
28. Springer, C. S. Measurement of metal cation compartmentalization in tissue by high-resolution metal cation NMR. *Annu. Rev. Biophys. Biophys. Chem.* **16**, 375–399 (1987).
29. Niesporek, S. C. *et al.* Partial volume correction for in vivo 23Na-MRI data of the human brain. *Neuroimage* **112**, 353–363 (2015).
30. Gnahm, C. & Nagel, A. M. Anatomically weighted second-order total variation reconstruction of 23Na MRI using prior information from 1H MRI. *Neuroimage* **105**, 452–461 (2015).
31. Niesporek, S. C. *et al.* Improved T2* determination in (23)Na, (35)Cl, and (17)O MRI using iterative partial volume correction based on (1)H MRI segmentation. *Magma N. Y. N.* https://doi.org/10.1007/s10334-017-0623-2 (2017).
32. Kim, S.-Y. *et al.* Voxel-wise partial volume correction method for accurate estimation of tissue sodium concentration in 23 Na-MRI at 7 T. *NMR Biomed.* **34**, e4448 (2021).
33. Lu, A., Atkinson, I. C., Claiborne, T. C., Damen, F. C. & Thulborn, K. R. Quantitative sodium imaging with a flexible twisted projection pulse sequence. *Magn. Reson. Med.* **63**, 1583–1593 (2010).
34. Thulborn, K. *et al.* Quantitative sodium MRI of the human brain at 9.4 T provides assessment of tissue sodium concentration and cell volume fraction during normal aging. *NMR Biomed.* **29**, 137–143 (2016).
35. Gilles, A., Nagel, A. M. & Madelin, G. Multipulse sodium magnetic resonance imaging for multicompartment quantification: Proof-of-concept. *Sci. Rep.* **7**, 17435 (2017).
36. Neeb, H., Schenk, J. & Weber, B. Multicentre absolute myelin water content mapping: Development of a whole brain atlas and application to low-grade multiple sclerosis. *NeuroImage Clin.* **1**, 121–130 (2012).
37. Filo, S. & Mezer, A. PD: Proton density of tissue water. In *Quantitative MRI of the Brain: Principles of Physical Measurement* 55–72 (CRC Press, 2018). https://doi.org/10.1201/b21837-4.

38. Herculano-Houzel, S. & Dos Santos, S. E. You do not mess with the glia. *Neuroglia* **1**, 193–219 (2018).
39. Dos Santos, S. E. *et al.* Similar microglial cell densities across brain structures and mammalian species: Implications for brain tissue function. *J. Neurosci. Off. J. Soc. Neurosci.* **40**, 4622–4643 (2020).
40. Harris, A. D., Puts, N. A. J., Barker, P. B. & Edden, R. A. E. Spectral-editing measurements of GABA in the human brain with and without macromolecule suppression. *Magn. Reson. Med.* **74**, 1523–1529 (2015).
41. Rooney, W. D. *et al.* Mapping human brain capillary water lifetime: high-resolution metabolic neuroimaging. *NMR Biomed.* **28**, 607–623 (2015).
42. Považan, M. *et al.* Simultaneous mapping of metabolites and individual macromolecular components via ultra-short acquisition delay 1 H MRSI in the brain at 7T. *Magn. Reson. Med.* **79**, 1231–1240 (2018).
43. Harrer, M., Cuijpers, P., Furukawa, T. A. & Ebert, D. D. *Doing Meta-Analysis with R: A Hands-On Guide* (Chapman & Hall/CRC Press, 2021).
44. Nichols, T. E. *et al.* Best practices in data analysis and sharing in neuroimaging using MRI. *Nat. Neurosci.* https://doi.org/10.1101/054262 (2016).
45. Winkler, S. S., Thomasson, D. M., Sherwood, K. & Perman, W. H. Regional T2 and sodium concentration estimates in the normal human brain by sodium-23 MR imaging at 1.5 T. *J. Comput. Assist. Tomogr.* **13**, 561–566 (1989).
46. Worthoff, W. A., Shymanskaya, A. & Shah, N. J. Relaxometry and quantification in simultaneously acquired single and triple quantum filtered sodium MRI. *Magn. Reson. Med.* **81**, 303–315 (2019).
47. Fleysher, L. *et al.* Noninvasive quantification of intracellular sodium in human brain using ultrahigh-field MRI. *NMR Biomed.* **26**, 9–19 (2013).
48. Syková, E. & Nicholson, C. Diffusion in brain extracellular space. *Physiol. Rev.* **88**, 1277–1340 (2008).
49. Madelin, G., Babb, J., Xia, D. & Regatte, R. R. Repeatability of quantitative sodium magnetic resonance imaging for estimating pseudo-intracellular sodium concentration and pseudo-extracellular volume fraction in brain at 3 T. *PLoS ONE* **10**, e0118692 (2015).
50. Knöpfel, T., Guatteo, E., Bernardi, G. & Mercuri, N. B. Hyperpolarization induces a rise in intracellular sodium concentration in dopamine cells of the substantia nigra pars compacta. *Eur. J. Neurosci.* **10**, 1926–1929 (1998).
51. Pisani, A., Calabresi, P., Tozzi, A., Bernardi, G. & Knöpfel, T. Early sodium elevations induced by combined oxygen and glucose deprivation in pyramidal cortical neurons. *Eur. J. Neurosci.* **10**, 3572–3574 (1998).
52. Rose, C. R. & Ransom, B. R. Intracellular sodium homeostasis in rat hippocampal astrocytes. *J. Physiol.* **491**(Pt 2), 291–305 (1996).
53. Rose, C. R. & Ransom, B. R. Gap junctions equalize intracellular Na+ concentration in astrocytes. *Glia* **20**, 299–307 (1997).
54. Unichenko, P., Myakhar, O. & Kirischuk, S. Intracellular Na+ concentration influences short-term plasticity of glutamate transporter-mediated currents in neocortical astrocytes. *Glia* **60**, 605–614 (2012).
55. El Mendili, M. M. *et al.* Alterations of microstructure and sodium homeostasis in fast amyotrophic lateral sclerosis progressors: A brain DTI and sodium MRI study. *AJNR Am. J. Neuroradiol.* **43**, 984–990 (2022).
56. Kolbe, S. C. *et al.* Microstructural correlates of 23Na relaxation in human brain at 7 Tesla. *Neuroimage* **211**, 116609 (2020).
57. Collorone, S. *et al.* Brain microstructural and metabolic alterations detected in vivo at onset of the first demyelinating event. *Brain J. Neurol.* https://doi.org/10.1093/brain/awab043 (2021).
58. Rodriguez, G. G. *et al.* Repeatability of simultaneous 3D 1H MRF/23Na MRI in brain at 7 T. *Sci. Rep.* **12**, 14156 (2022).
59. Schneider, T. M. *et al.* Multiparametric MRI for characterization of the basal ganglia and the midbrain. *Front. Neurosci.* https://doi.org/10.3389/fnins.2021.661504 (2021).
60. Niesporek, S. C., Nagel, A. M. & Platt, T. Multinuclear MRI at ultrahigh fields. *Top. Magn. Reson. Imaging* **28**, 173–188 (2019).
61. Adlung, A. *et al.* Quantification of tissue sodium concentration in the ischemic stroke: A comparison between external and internal references for 23Na MRI. *J. Neurosci. Methods* **382**, 109721. https://doi.org/10.1016/j.jneumeth.2022.109721 (2022).
62. Thulborn, K. R. Gender differences in cell volume fraction (CVF): a structural parameter reflecting the energy efficiency of maintaining the resting membrane potential. *NMR Biomed.* **35**, e4693 (2022).
63. Ridley, B. *et al.* Distribution of brain sodium long and short relaxation times and concentrations: a multi-echo ultra-high field 23Na MRI study. *Sci. Rep.* **8**, 4357 (2018).
64. Nagel, A. M. *et al.* The potential of relaxation-weighted sodium magnetic resonance imaging as demonstrated on brain tumors. *Invest. Radiol.* **46**, 539–547 (2011).
65. Burstein, D. & Springer, C. S. Sodium MRI revisited. *Magn. Reson. Med.* **82**, 521–524 (2019).
66. Hutchison, R. B. & Shapiro, J. I. Measurement of intracellular sodium with NMR methods. *Concepts Magn. Reson.* **3**, 215–236 (1991).
67. Hoesl, M. A. U. *et al.* 23 Na Triple-quantum signal of in vitro human liver cells, liposomes, and nanoparticles: Cell viability assessment vs. separation of intra- and extracellular signal. *J. Magn. Reson. Imaging JMRI* https://doi.org/10.1002/jmri.26666 (2019).
68. Inglese, M., Oesingmann, N., Zaaraoui, W., Ranjeva, J. P. & Fleysher, L. Sodium imaging as a marker of tissue injury in patients with multiple sclerosis. *Mult. Scler. Relat. Disord.* **2**, 263–269 (2013).
69. Paling, D., Golay, X., Wheeler-Kingshott, C., Kapoor, R. & Miller, D. Energy failure in multiple sclerosis and its investigation using MR techniques. *J. Neurol.* **258**, 2113–2127 (2011).
70. Petracca, M., Fleysher, L., Oesingmann, N. & Inglese, M. Sodium MRI of multiple sclerosis. *NMR Biomed.* **29**, 153–161 (2016).
71. Qian, Y., Zhao, T., Zheng, H., Weimer, J. & Boada, F. E. High-resolution sodium imaging of human brain at 7 T. *Magn. Reson. Med.* **68**, 227–233 (2012).
72. Riemer, F. *et al.* Measuring tissue sodium concentration: Cross-vendor repeatability and reproducibility of 23 Na-MRI across two sites. *J. Magn. Reson. Imaging JMRI* **50**, 1278–1284 (2019).
73. Mirkes, C. C., Hoffmann, J., Shajan, G., Pohmann, R. & Scheffler, K. High-resolution quantitative sodium imaging at 9.4 Tesla. *Magn. Reson. Med.* **73**, 342–351 (2015).
74. Viechtbauer, W. Conducting meta-analyses in R with the metafor package. *J. Stat. Softw.* **36**, 1–48 (2010).
75. Viechtbauer, W. Bias and efficiency of meta-analytic variance estimators in the random-effects model. *J. Educ. Behav. Stat.* **30**, 261–293 (2005).
76. Knapp, G. & Hartung, J. Improved tests for a random effects meta-regression with a single covariate. *Stat. Med.* **22**, 2693–2710 (2003).
77. Pustejovsky, J. E. & Tipton, E. Meta-analysis with robust variance estimation: Expanding the range of working models. *Prev. Sci.* **23**, 425–438 (2022).
78. Pustejovsky, J. clubSandwich: Cluster-Robust (Sandwich) Variance Estimators with Small-Sample Corrections. (2022). https://CRAN.R-project.org/package=clubSandwich.
79. Egger, M., Davey Smith, G., Schneider, M. & Minder, C. Bias in meta-analysis detected by a simple, graphical test. *BMJ* **315**, 629–634 (1997).
80. Springer, C. S. Biological systems: Spin-3/2 nuclei. In *eMagRes* (American Cancer Society, 2007). https://doi.org/10.1002/9780470034590.emrstm0029.
81. Woessner, D. E. NMR relaxation of spin-3/2 nuclei: Effects of structure, order, and dynamics in aqueous heterogeneous systems. *Concepts Magn. Reson.* **13**, 294–325 (2001).
82. Eliav, U. & Navon, G. Sodium NMR/MRI for anisotropic systems. *NMR Biomed.* **29**, 144–152 (2016).

83. Haddaway, N. R., Page, M. J., Pritchard, C. C. & McGuinness, L. A. PRISMA2020: An R package and Shiny app for producing PRISMA 2020-compliant flow diagrams, with interactivity for optimised digital transparency and Open Synthesis. *Campbell Syst. Rev.* **18**, e1230 (2021).
84. R Core Team. R: A language and environment for statistical computing. (2021).
85. Wickham, H. *et al.* Welcome to the Tidyverse. *J. Open Source Softw.* **4**, 1686 (2019).
86. Wickham, H. *et al.* ggplot2: Create Elegant Data Visualisations Using the Grammar of Graphics. (2021).
87. Thulborn, K. R., Davis, D., Snyder, J., Yonas, H. & Kassam, A. Sodium MR imaging of acute and subacute stroke for assessment of tissue viability. *Neuroimaging Clin. N. Am.* **15**(639–653), xi–xii (2005).
88. Niesporek, S. C. *et al.* Partial volume correction for in vivo (23)Na-MRI data of the human brain. *Neuroimage* **112**, 353–363 (2015).
89. Driver, I. D., Stobbe, R. W., Wise, R. G. & Beaulieu, C. Venous contribution to sodium MRI in the human brain. *Magn. Reson. Med.* **83**, 1331–1338 (2020).
90. Liao, Y. *et al.* Correlation of quantitative conductivity mapping and total tissue sodium concentration at 3T/4T. *Magn. Reson. Med.* **82**, 1518–1526 (2019).
91. Meyer, M. M. *et al.* Repeatability and reproducibility of cerebral 23Na imaging in healthy subjects. *BMC Med. Imaging* **19**, 26 (2019).
92. Gerhalter, T. *et al.* Global decrease in brain sodium concentration after mild traumatic brain injury. *Brain Commun.* **3**, fcabo51 (2021).

Author contributions

B.R. conceived and planned the work, designed, and ran the literature search. B.R., W.Z. and F.N. contributed to data extraction. B.R. and F.M. designed and ran the analysis and prepared figures. All authors contributed to interpretation of the results. B.R. drafted the manuscript, which was revised by all authors, who agreed to the final version.

Competing interests

The authors declare no competing interests.

Additional information

Supplementary Information The online version contains supplementary material available at https://doi.org/10.1038/s41598-023-30363-y.

Correspondence and requests for materials should be addressed to B.R.

Reprints and permissions information is available at www.nature.com/reprints.

Publisher's note Springer Nature remains neutral with regard to jurisdictional claims in published maps and institutional affiliations.